Earthquakes and Structures, *Vol. 13, No. 6 (2017) 573-588*
DOI: https://doi.org/10.12989/eas.2017.13.6.573

Obliquely incident earthquake for soil-structure interaction in layered half space

Mi Zhao[1,2], Zhidong Gao[1,2], Litao Wang[1,2], Xiuli Du[*1,2], Jingqi Huang[1,2] and Yang Li[1,2]

[1]*Key Laboratory of Urban Security and Disaster Engineering of Ministry of Education, Beijing University of Technology, Beijing 100124, China*
[2]*Beijing Collaborative Innovation Center for Metropolitan Transportation, Beijing University of Technology, Beijing 100124, China*

(Received March 25, 2017, Revised December 10, 2017, Accepted January 16, 2018)

Abstract. The earthquake input is required when the soil-structure interaction (SSI) analysis is performed by the direct finite element method. In this paper, the earthquake is considered as the obliquely incident plane body wave arising from the truncated linearly elastic layered half space. An earthquake input method is developed for the time-domain three-dimensional SSI analysis. It consists of a new site response analysis method for free field and the viscous-spring artificial boundary condition for scattered field. The proposed earthquake input method can be implemented in the process of building finite element model of commercial software. It can result in the highly accurate solution by using a relatively small SSI model. The initial condition is considered for the nonlinear SSI analysis. The Daikai subway station is analyzed as an example. The effectiveness of the proposed earthquake input method is verified. The effect of the obliquely incident earthquake is studied.

Keywords: seismic soil-structure interaction; layered half space; oblique incidence; artificial boundary condition; site response analysis

1. Introduction

The soil-structure interaction (SSI) affects the seismic response of many civil infrastructures, such as underground structures, high dams, nuclear power plants, large-span bridges and so on. The framework of direct method (Wolf 1985, 1988) has been proposed for the seismic SSI analysis based on the finite element modeling. The earthquake input is required at the truncation boundary called artificial boundary of the finite element model. It consists of the site response analysis to obtain the free field and the artificial boundary condition to absorb the scattered field. Some professional programs (Lysmer *et al*. 1975, 2000, Lysmer *et al*. 2000, Hudson *et al*. 2003) and the implementation into a commercial finite element software such as ABAQUS® (Nielsen 2006) have been developed for the direct method. Many works (An *et al*. 1997a, Parra-Montesinos *et al*. 2006, Chen *et al*. 2010, Saouma *et al*. 2011, Ghandil and Behnamfar 2015, Zhuang *et al*. 2015) have been done to apply the direct method to perform the seismic SSI analysis.

The above works consider the earthquakes as the plane body waves of vertical incidence. This assumption is usually applicable to the relatively deep focus earthquake or to the engineering site near the epicenter. However, for a shallow focus earthquake and when the engineering site moderately far from the epicenter, the oblique incidence of the earthquake as the plane body wave should be considered.

The site response analysis from the obliquely incident earthquake solves in nature the two-dimensional problem in unbounded domain. The frequency-domain analytical methods such as the transfer matrix method (Thomson 1950, Haskell 1951) and the stiffness matrix method (Kausel and Roesset 1981, Wolf and Obernhuber 1982a, b, 1983, Takano *et al*. 1988) have been developed. The direct and inverse Fourier transforms are used for the time-domain analysis. It can be seen such as in this paper that the frequency-domain method with Fourier transform may result in the inaccurate response. A time-domain numerical method (Liu and Wang 2006, 2007) has been proposed to avoid this problem. In this numerical method the viscous boundary (Lysmer 1969) is used to model the wave absorption of the truncated underlying half space. The finite element method with the central difference time integration algorithm is applied directly to the two-dimensional problem of spatial-infinity along the layer direction. Snell's law is then used to transform the two-dimensional discrete problem into the one-dimensional one. In this method the viscous boundary is an approximate treatment to the P-SV wave case, leading to the responses of low accuracy. P represents the primary or pressure wave. SV represents the secondary or shear wave. On the other hand, this method has a stability limitation on the time integration step size. The above time-domain numerical method is modified in two aspects (Zhao *et al*. 2015). An accurate boundary condition is developed to replace the viscous boundary. Snell's law is used in the spatially continuous case to transform the two-dimensional problem to one dimension. The finite element method is then used to discretize the resulting one-dimensional problem.

The artificial boundary condition is a numerical method in many fields of science and engineering. A large number of artificial boundary conditions has been developed in the last six decades. The early artificial boundary conditions include the viscous boundary (Lysmer 1969), the viscous-spring boundary (Deeks and Randolph 1994, Du *et*

*Corresponding author, Professor
E-mail: zhaomi@bjut.edu.cn

ISSN: 2092-7614 (Print), 2092-7622 (Online)

al. 2006, Liu *et al*. 2006, Du and Zhao 2010), the extrapolation boundary (Liao and Wong 1984, Liao 1996), the infinite element method (Zhao 2009), the boundary element method (Hall and Oliveto 2009, Galvín and Romero 2014) and the boundary element and infinite element coupling (Zhang *et al*. 1999). The further developments include the perfectly matched layer (Berenger 1994), the Dirichlet-to-Neumann (DtN) method (Givoli 1999, Du and Zhao 2010, Zhao 2011), the high-order local non-reflecting boundary condition (Givoli 2004), the scaled boundary finite element method (Song and Wolf 1997, Zhang *et al*. 1999, Wolf, 2003, Birk and Behnke 2012, Chen *et al*. 2015). The viscous and viscous-spring boundaries are easily coupled with the finite element method and are stable and efficient, although they are approximate.

In this paper, three-dimensional SSI problem is analyzed in time domain by using the commercial finite element software ABAQUS® (1998). The earthquake as the plane body wave is obliquely incident from the linearly elastic layered half space. The earthquake input method is developed. An easy-to-understand mechanic derivation is given for the site response analysis method (Zhao *et al*. 2015). The viscous and viscous-spring artificial boundary conditions are proved to have the sufficient accuracy for the seismic SSI.

The resting parts of this paper are organized as follows. The direct method to solve the seismic SSI problem is summarized in Section 2. The finite element model for the soil-structure system of Daikai subway station is illustrated in Section 3. The model for the obliquely incident earthquake is given in Section 4. The earthquake input method is developed in Section 5. The method is verified in Section 6. The effect of the obliquely incident earthquake on the response of Daikai subway station system is studied in Section 7. Conclusions follow in Section 8.

2. Direct method for seismic soil-structure interaction

The seismic SSI problem is shown in Fig. 1(a). An artificial boundary is introduced to divide the soil-structure system into the finite and infinite domains. The finite domain contains the structure and its adjacent soil. It is modeled by the finite element method. After the spatial discretization the finite element equation of the finite domain is

$$\begin{bmatrix}\mathbf{M}_{RR} & \mathbf{M}_{RB}\\ \mathbf{M}_{BR} & \mathbf{M}_{BB}\end{bmatrix}\begin{Bmatrix}\ddot{\mathbf{u}}_R\\ \ddot{\mathbf{u}}_B\end{Bmatrix}+\begin{bmatrix}\mathbf{C}_{RR} & \mathbf{C}_{RB}\\ \mathbf{C}_{BR} & \mathbf{C}_{BB}\end{bmatrix}\begin{Bmatrix}\dot{\mathbf{u}}_R\\ \dot{\mathbf{u}}_B\end{Bmatrix}+\begin{bmatrix}\mathbf{K}_{RR} & \mathbf{K}_{RB}\\ \mathbf{K}_{BR} & \mathbf{K}_{BB}\end{bmatrix}\begin{Bmatrix}\mathbf{u}_R\\ \mathbf{u}_B\end{Bmatrix}=\begin{Bmatrix}\mathbf{0}\\ \mathbf{f}_B\end{Bmatrix} \tag{1}$$

where the subscripts B and R denote the degrees of freedom on artificial boundary and the rest of the finite domain, respectively; $\mathbf{u}$, $\dot{\mathbf{u}}$ and $\ddot{\mathbf{u}}$ are the absolute displacement, velocity and acceleration vectors, respectively; $\mathbf{M}$, $\mathbf{C}$ and $\mathbf{K}$ are the mass, damping and stiffness matrices, respectively; and $\mathbf{f}_B$ is the action force vector of the infinite domain to the finite domain. The finite domain is initially resting. Although the linear elastic finite element equation is written in Eq. (1) for simplicity, the finite domain may contain the possible material, geometry and contact nonlinearities.

The infinite domain is usually assumed as the linearly elastic layered half space with an excavation. The infinite domain is truncated but its earthquake input and radiation damping effects should be considered. The response of the infinite domain can be decomposed into the scattered and free fields. It can be written at the artificial boundary as

$$\mathbf{f}_B=\mathbf{f}_B^S+\mathbf{f}_B^F \tag{2}$$

$$\mathbf{u}_B=\mathbf{u}_B^S+\mathbf{u}_B^F \quad \text{and} \quad \dot{\mathbf{u}}_B=\dot{\mathbf{u}}_B^S+\dot{\mathbf{u}}_B^F \tag{3}$$

where the superscripts S and F denote the scattered and free fields, respectively. The seismic free field can be obtained by performing a site response analysis before the SSI analysis. The site under earthquake is the linearly elastic layered half space subjected to the obliquely incident plane body wave.

The scattered field is absorbed by an artificial boundary condition imposed on the artificial boundary of the finite domain. The viscous boundary (Lysmer 1969) is the well-known artificial boundary condition. To avoid the low-frequency instability due to the absence of stiffness in the viscous boundary, the viscous-spring boundary has been developed (Deeks and Randolph 1994, Liu *et al*. 2006, Du *et al*. 2006, Du and Zhao 2010). The viscous boundary is a special case of the viscous-spring boundary with zero stiffness. The viscous-spring boundary is obtained from the one-dimensional wave motion theory, and has been applied approximately to the two- and three-dimensional wave problems. The formulation of the viscous-spring boundary can be written as

$$\mathbf{f}_B^S=-\mathbf{K}_B^\infty\mathbf{u}_B^S-\mathbf{C}_B^\infty\dot{\mathbf{u}}_B^S \tag{4}$$

where $\mathbf{K}_B^\infty$ and $\mathbf{C}_B^\infty$ are the stiffness and damping matrices, respectively. If the spatially lumped discretization is used, both the stiffness and damping matrices are diagonal. The viscous-spring boundary is a parallel spring-dashpot model for each degree of freedom on the artificial boundary.

Substituting Eq. (3) into Eq. (4) and then into Eq. (2) and finally into Eq. (1), after some manipulations, obtain the finite element equation as

$$\begin{bmatrix}\mathbf{M}_{RR} & \mathbf{M}_{RB}\\ \mathbf{M}_{BR} & \mathbf{M}_{BB}\end{bmatrix}\begin{Bmatrix}\ddot{\mathbf{u}}_R\\ \ddot{\mathbf{u}}_B\end{Bmatrix}+\begin{bmatrix}\mathbf{C}_{RR} & \mathbf{C}_{RB}\\ \mathbf{C}_{BR} & \mathbf{C}_{BB}+\mathbf{C}_B^\infty\end{bmatrix}\begin{Bmatrix}\dot{\mathbf{u}}_R\\ \dot{\mathbf{u}}_B\end{Bmatrix}+\begin{bmatrix}\mathbf{K}_{RR} & \mathbf{K}_{RB}\\ \mathbf{K}_{BR} & \mathbf{K}_{BB}+\mathbf{K}_B^\infty\end{bmatrix}\begin{Bmatrix}\mathbf{u}_R\\ \mathbf{u}_B\end{Bmatrix}=\begin{Bmatrix}\mathbf{0}\\ \mathbf{f}_B^\infty\end{Bmatrix} \tag{5}$$

with the seismic load

$$\mathbf{f}_B^\infty=\mathbf{K}_B^\infty\mathbf{u}_B^F+\mathbf{C}_B^\infty\dot{\mathbf{u}}_B^F+\mathbf{f}_B^F \tag{6}$$

where the seismic load is nodal force arising from the free field response.

Eqs. (5) and (6) represent the direct method for the seismic SSI analysis. As shown in Fig. 1(b), it can be

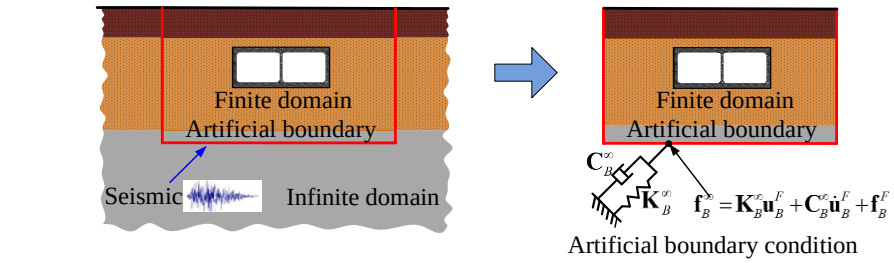

(a) Seismic soil-structure interaction problem (b) Direct method

Fig. 1 Direct method for seismic soil-structure interaction

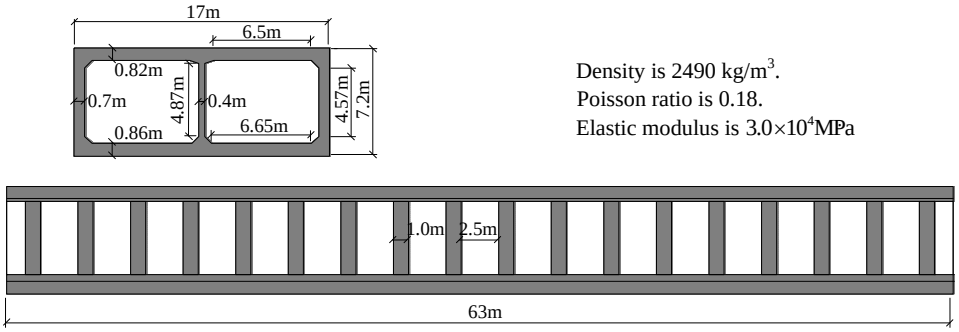

Fig. 2 Geometry and material constants of structure

implemented in the preprocessing of the commercial finite element software. The process is as follows.

First, building the finite element model of the finite domain in the preprocessing of the commercial software. This gives the left hand side of Eq. (5) without the stiffness and damping matrices of artificial boundary condition. The Daikai subway station is considered in Section 3.

Second, giving the incident earthquake model. The earthquake is considered as the plane body wave of oblique incidence. The definition is given in Section 4.

Third, inputting the given earthquake into the finite element model. The earthquake input is to apply the viscous-spring boundary and seismic load on the artificial boundary of the finite element model. This gives the stiffness and damping matrices of artificial boundary condition on the left hand side of Eq. (5) and the seismic load on the right hand side of Eq. (5), respectively. The earthquake input can be implemented in the preprocessing of the commercial software. The implementation does not require any modification of the finite element codes. The key of this step is to obtain the free field response by the seismic site response analysis and to give the stiffness and damping matrices of the viscous-spring boundary before the seismic SSI analysis. The two issues are discussed in Section 5.

Fourth, solving Eq. (5) by the time integration algorithm. This is done by using the time integration solver in the commercial software, such as the widely used Newmark method.

3. Finite element model

The Daikai subway station in Japan is studied as an example in this paper. The geometry and material constants of the structure are shown in Fig. 2. The burial depth of the underground structure is 4.8 m that is the distance from the horizontal ground surface to the top of structure.

Table 1 Geometry and material constants of soil

Layer number	Depth (m)	Density (kg/m^3)	Elastic modulus (MPa)	Poisson ratio
1	0-1.0	1900	99.3	0.333
2	1.0-5.1	1900	110.0	0.488
3	5.1-8.3	1900	164.0	0.493
4	8.3-11.5	1900	204.0	0.494
5	11.5-17.3	1900	326.0	0.490
6	17.3-39.3	2000	648.0	0.487
7	39.3-∞	2100	1540.0	0.470

The soil is a horizontally layered half space. The geometry and material constants of the soil site are listed in Table 1. The continuity condition is satisfied at the interface between two soil layers.

The finite element model of the soil-structure system is shown in Fig. 3. The continuity condition is satisfied at the interface between soil and structure. An artificial boundary is introduced into the soil to truncate the infinite domain. The three-dimensional artificial boundary consists of the five surfaces of cuboid where the outward normal of each surface is parallel to an axis of global coordinate (x,y,z). Both the length and width of the finite element model are 70 m, and the depth is 40.3 m. It can be seen from the numerical example in Section 6 that such relatively small finite domain can obtain the accurate solution to the seismic SSI analysis. The finite element mesh size satisfies the requirement for the dynamic analysis. For three-dimensional finite element model, the number of the finite elements is 216048, and the number of nodes is 244332.

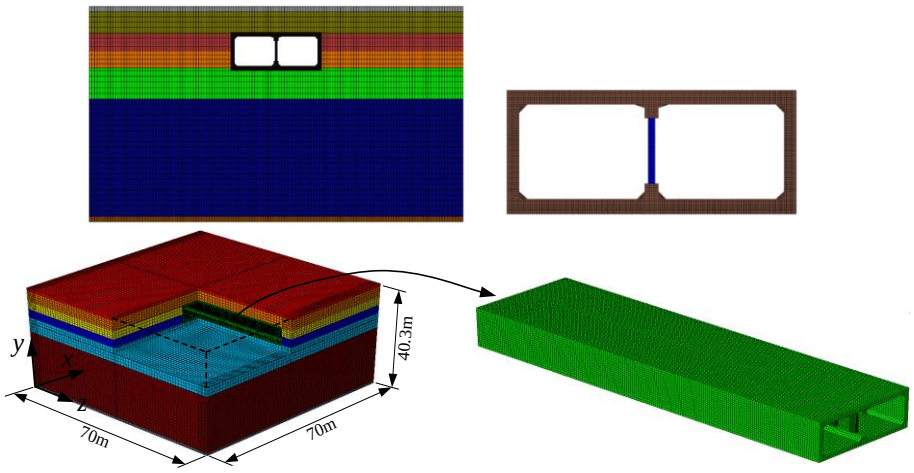

Fig. 3 Finite element model of soil-structure system

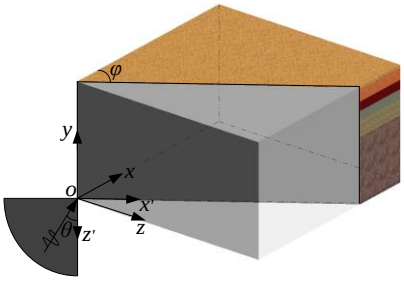

(a) Three-dimensional view

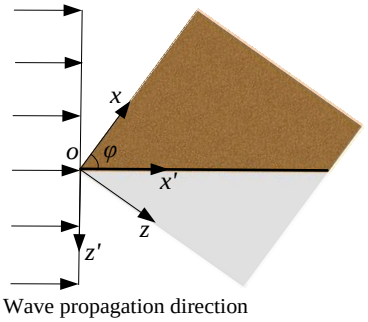

(b) Top view

Fig. 4 Sketch map for obliquely incident earthquake inputted into site response or soil-structure system

4. Obliquely incident earthquake

The earthquake is the obliquely incident plane body wave from the underlying half space. The global coordinate (x,y,z) is located on the artificial boundary of the soil-structure system, as shown in Fig. 4. The earthquake is inputted from the coordinate origin. A local coordinate (x',y,z') is introduced to illustrate the incident wave direction. The $x'oy$ plane is parallel to the wave propagation direction. The θ is the angle between the wave propagation direction and the y axis. The φ is the angle between the x and x' axes.

The three kinds of plane body waves are defined as follows. The *P* wave has the vibration direction along the wave propagation direction. The *SV* wave has the vibration direction perpendicular to the wave propagation direction and parallel to the $x'oy$ plane. The *SH* wave has the vibration direction perpendicular to the $x'oy$ plane. The time history of the incident earthquake at the coordinate origin is chosen as a half of the record at Kobe Maritime Observatory, as shown in Fig. 5.

5. Earthquake input method

5.1 Seismic site response

The free field response is obtained by the seismic site response analysis. The site is the linearly elastic layered half space. The site response analysis under the obliquely incident earthquake solves the two-dimensional problem in the $x'oy$ plane, as shown in Fig. 4. It consists of the in-plane problem under the incident *P* or *SV* wave and the out-of-plane problem under the incident *SH* wave. A time-domain numerical method (Zhao *et al*. 2015) has been proposed for the site response analysis from the obliquely incident *P-SV* waves. This method obtains the one-dimensional site response along the y axis. In this paper, a new mechanic derivation is given in Subsection 5.1.1. According to the similar derivation, the method for the obliquely incident SH wave is given in Subsection 5.1.2. The resulting one-dimensional site responses in the local coordinate (x',y,z') are extended in Subsection 5.1.3 to the three dimensions in the global coordinate (x,y,z) including each finite element node on the artificial boundary.

5.1.1 One-dimensional response in local coordinate from P-SV waves

First, the underlying half space of the layered half space site is truncated. A boundary condition is developed and imposed on the truncation boundary of the residual layered site. The boundary condition is a relationship between the stress and velocity on the truncation boundary. It can be written as (Zhao *et al*. 2015)

$$\boldsymbol{\sigma}_I = \mathbf{S}\dot{\mathbf{u}}_I(\mathbf{R}-\mathbf{S})\dot{\hat{\mathbf{u}}}_I \tag{7}$$

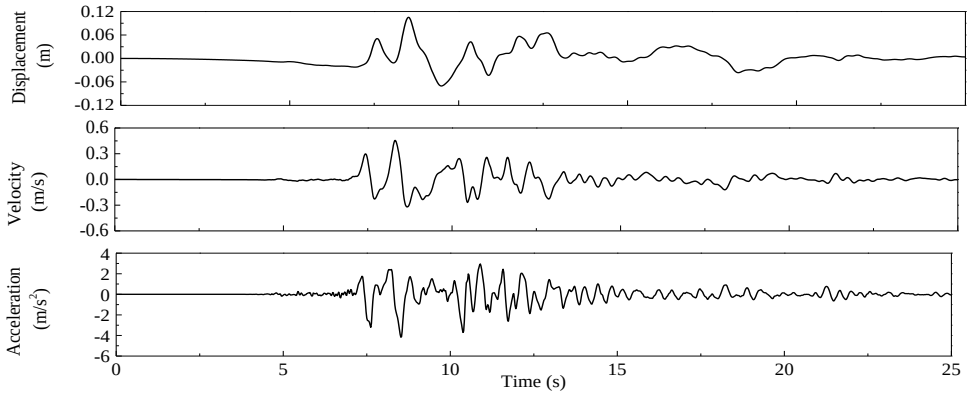

Fig. 5 Time histories of incident earthquake (An *et al*. 1997b)

With

$$\mathbf{S}=-\frac{1}{c_{x'}}\begin{bmatrix}-2Gm_Pn_P & G(m_S^2-n_S^2)\\ \lambda+2Gn_P^2 & -2Gm_Sn_S\end{bmatrix}\begin{bmatrix}m_P^2 & m_Sn_S\\ -m_Pn_P & m_S^2\end{bmatrix}^{-1} \tag{8}$$

$$\mathbf{R}=\begin{cases}-\dfrac{1}{c_P}\begin{Bmatrix}2Gm_Pn_P\\ \lambda+2Gn_P^2\end{Bmatrix}\{m_P\ \ n_P\}\\ \text{for P wave incidence}\\ -\dfrac{1}{c_S}\begin{Bmatrix}G(m_S^2-n_S^2)\\ 2Gm_Sn_S\end{Bmatrix}\{-n_S\ \ m_S\}\\ \text{for SV wave incidence}\end{cases} \tag{9}$$

$$m_P=\frac{c_P}{c_{x'}}\ ,\quad n_S=\sqrt{1-\left(\frac{c_S}{c_{x'}}\right)^2}\ ,\quad m_S=\frac{c_S}{c_{x'}}\ \text{and}\ \ n_P=\sqrt{1-\left(\frac{c_P}{c_{x'}}\right)^2} \tag{10}$$

$$c_{x'}=\begin{cases}\dfrac{c_P}{\sin\theta} & \text{for P wave incidence}\\ \dfrac{c_S}{\sin\theta} & \text{for SV wave incidence}\end{cases} \tag{11}$$

$$\dot{\hat{\mathbf{u}}}_I=\begin{cases}\{\sin\theta\ \ \cos\theta\}^T\dot{u}_{P0}\\ \text{for P wave incidence}\\ \{\cos\theta\ \ -\sin\theta\}^T\dot{u}_{SV0}\\ \text{for SV wave incidence}\end{cases} \tag{12}$$

where $\boldsymbol{\sigma}_I=\{\tau_{x'y}\ \ \sigma_y\}^T$ and $\dot{\hat{\mathbf{u}}}_I=\{\dot{u}_{x'}\ \ \dot{u}_y\}^T$ are the stress and velocity vectors on the truncation boundary, respectively; λ and G are the Lame constants of the underlying half space; c_P and c_S are the P and S wave velocities of the underlying half space, respectively; $c_{x'}$ is the apparent wave velocity of the plane body wave along the x'-axis direction; and $\dot{u}_{P0}$ and $\dot{u}_{SV0}$ are the time histories of the known incident plane P and SV waves on the truncation boundary, respectively.

Second, the residual layered site is discretized only along the y direction by using the finite elements. This is similar to the thin layer method (Sun 2013, Kausel 1994). The resulting equation is

$$\mathbf{B}_1\frac{\partial^2\mathbf{u}}{\partial x'^2}+\mathbf{B}_2\frac{\partial\mathbf{u}}{\partial x'}-\mathbf{B}_3\mathbf{u}+\boldsymbol{\sigma}=\mathbf{B}_4\ddot{\mathbf{u}} \tag{13}$$

with the displacement and stress vectors, respectively

$$\mathbf{u}=\begin{Bmatrix}\mathbf{u}_I\\ \mathbf{u}_L\end{Bmatrix}\ \text{and}\ \ \boldsymbol{\sigma}=\begin{Bmatrix}-\boldsymbol{\sigma}_I\\ \mathbf{0}\end{Bmatrix} \tag{14}$$

and the matrices $\mathbf{B}_1$, $\mathbf{B}_2$, $\mathbf{B}_3$ and $\mathbf{B}_4$ assembled from the following element matrices, respectively

$$\mathbf{B}_1^e=\frac{\Delta y}{6}\begin{bmatrix}2(\lambda_j+2G_j) & 0 & \lambda_j+2G_j & 0\\ 0 & 2G_j & 0 & G_j\\ \lambda_j+2G_j & 0 & 2(\lambda_j+2G_j) & 0\\ 0 & G_j & 0 & 2G_j\end{bmatrix} \tag{15}$$

$$\mathbf{B}_2^e=\frac{1}{2}\begin{bmatrix}0 & G_j-\lambda_j & 0 & \lambda_j+G_j\\ \lambda_j-G_j & 0 & \lambda_j+G_j & 0\\ 0 & -(\lambda_j+G_j) & 0 & \lambda_j-G_j\\ -(\lambda_j+G_j) & 0 & G_j-\lambda_j & 0\end{bmatrix} \tag{16}$$

$$\mathbf{B}_3^e=\frac{1}{\Delta y}\begin{bmatrix}G_j & 0 & -G_j & 0\\ 0 & \lambda_j+2G_j & 0 & -(\lambda_j+2G_j)\\ -G_j & 0 & G_j & 0\\ 0 & -(\lambda_j+2G_j) & 0 & \lambda_j+2G_j\end{bmatrix} \tag{17}$$

$$\mathbf{B}_4^e=\frac{\rho_j\Delta y}{6}\begin{bmatrix}2 & 0 & 1 & 0\\ 0 & 2 & 0 & 1\\ 1 & 0 & 2 & 0\\ 0 & 1 & 0 & 2\end{bmatrix} \tag{18}$$

where the superscripts I and L denote the degrees of freedom on the truncation boundary and the resting ones, respectively; Δy is the element length; and ρ_j, λ_j and G_j are

the density and the Lame constants of the *j*-th element, respectively.

Third, Eq. (13) is transformed into the one dimension by using Snell's law. The Snell's law leads to the differential relation

$$\frac{\partial}{\partial x'} = -\frac{1}{c_{x'}}\frac{\partial}{\partial t} \tag{19}$$

Substituting Eq. (7) into Eq. (13) and applying Eq. (19) to the result, after some manipulations, lead to the dynamic equation only along *y* coordinate as

$$\mathbf{M}\ddot{\mathbf{u}} + \left(\mathbf{C} + \mathbf{C}_B\right)\dot{\mathbf{u}} + \mathbf{K}\mathbf{u} = \mathbf{f} \tag{20}$$

with the mass matrix, the damping matrix, the stiffness matrix, the boundary damping matrix and the boundary force vector, respectively, as

$$\begin{aligned} &\mathbf{M} = \mathbf{B}_4 - \frac{\mathbf{B}_1}{c_{x'}^2}\ ,\ \mathbf{C} = \frac{\mathbf{B}_2}{c_{x'}}\ ,\mathbf{K} = \mathbf{B}_3 \\ &\mathbf{C}_B = \begin{bmatrix} \mathbf{S} & \mathbf{0} \\ \mathbf{0} & \mathbf{0} \end{bmatrix} \text{ and } \mathbf{f} = \begin{Bmatrix} (\mathbf{S}-\mathbf{R})\,\dot{\mathbf{u}}_I \\ \mathbf{0} \end{Bmatrix} \end{aligned} \tag{21}$$

Eq. (20) can be solved by the standard time integration algorithm in structural dynamics, such as Newmark method. The displacement, velocity and acceleration of the site along the *y* coordinate are obtained.

Finally, the stress is computed. The stresses $\tau_{x'y}$ and σ_y can be obtained by the dynamic equation of each finite element from the known motions obtained above. The stresses $\sigma_{x'}$ and $\sigma_{z'}$ can be then obtained from the stress-displacement relationship where $\partial u_y/\partial y$ is eliminated by the σ_y-displacement relationship and $\partial u_{x'}/\partial x'$ is eliminated by Eq. (19).

5.1.2 One-dimensional response in local coordinate from SH wave

The boundary condition to replace the truncated underlying half space is

$$\tau_{yz',I} = \rho c_S \cos\theta\left(\dot{u}_{z',I} - 2\dot{u}_{SH0}\right) \tag{22}$$

where $\tau_{yz',I}$ and $\dot{u}_{z',I}$ are the stress and velocity on the truncation boundary, respectively; ρ and c_S are the density and *S* wave velocity of the underlying half space, respectively; and $\dot{u}_{SH0}$ is the time histories of the known incident plane SH wave on the truncation boundary.

The finite element equation of the residual layered site discretized along the *y* direction is

$$\mathbf{B}_1\frac{\partial^2\mathbf{u}}{\partial x'^2} - \mathbf{B}_2\mathbf{u} + \boldsymbol{\sigma} = \mathbf{B}_3\ddot{\mathbf{u}} \tag{23}$$

with the displacement and stress vectors, respectively

$$\mathbf{u} = \begin{Bmatrix} \dot{u}_{z',I} \\ \mathbf{u}_L \end{Bmatrix} \text{ and } \boldsymbol{\sigma} = \begin{Bmatrix} -\tau_{yz',I} \\ \mathbf{0} \end{Bmatrix} \tag{24}$$

and the matrices $\mathbf{B}_1$, $\mathbf{B}_2$ and $\mathbf{B}_3$ assembled from the element matrices, respectively

$$\begin{aligned} &\mathbf{B}_1^e = \frac{\Delta y G_j}{6}\begin{bmatrix} 2 & 1 \\ 1 & 2 \end{bmatrix}\ ,\ \mathbf{B}_2^e = \frac{G_j}{\Delta y}\begin{bmatrix} 1 & -1 \\ -1 & 1 \end{bmatrix} \\ &\text{and } \mathbf{B}_3^e = \frac{\Delta y \rho_j}{6}\begin{bmatrix} 2 & 1 \\ 1 & 2 \end{bmatrix} \end{aligned} \tag{25}$$

where the superscripts *I* and *L* denote the degrees of freedom on the truncation boundary and the resting ones, respectively; Δy is the element length; and ρ_j and G_j are the density and the shear modulus of the *j*-th element, respectively.

The dynamic equation along *y* coordinate is

$$\mathbf{M}\ddot{\mathbf{u}} + \mathbf{C}_B\dot{\mathbf{u}} + \mathbf{K}\mathbf{u} = \mathbf{f} \tag{26}$$

with the mass matrix, the stiffness matrix, the boundary damping matrix and the boundary force vector, respectively, as

$$\begin{aligned} &\mathbf{M} = \mathbf{B}_3 - \frac{\mathbf{B}_1}{c_{x'}^2}\ ,\ \mathbf{K} = \mathbf{B}_2\,, \\ &\mathbf{C}_B = \begin{bmatrix} \rho c_S\cos\theta & \mathbf{0} \\ \mathbf{0} & \mathbf{0} \end{bmatrix} \text{ and } \mathbf{f} = \begin{Bmatrix} 2\rho c_S\cos\theta\,\dot{u}_{SH0} \\ \mathbf{0} \end{Bmatrix} \end{aligned} \tag{27}$$

The stress computation is similar to that in the P-SV wave case.

5.1.3 Three-dimensional response in global coordinate

Snell's law means that the plane wave propagates along x' axis with the constant velocity $c_{x'}$, as shown in Figure 4b. The three-dimensional site response on the artificial boundary can therefore be obtained from the above one-dimensional response. The displacement vector of the node *i* on the artificial boundary can be written in the local coordinate (x', y, z') as

$$\begin{aligned} &\mathbf{u}_{Bi}^{F(1)}(x_i', y_i, z_i', t) = \begin{cases} \mathbf{0} & 0 \le t \le t_i \\ \mathbf{u}_j(0, y_i, 0, t - t_i) & t > t_i \end{cases} \\ &\text{with } t_i = \frac{\left|x_i'\cos\varphi + z_i'\sin\varphi\right|}{c_{x'}} \end{aligned} \tag{28}$$

where $\mathbf{u}_{Bi}^{F(1)}$ is the displacement of the node *i*; $\mathbf{u}_j$ is the obtained displacement of the node *j* on *y* axis; the local coordinates of the nodes *i* and *j* are (x'_i, y_i, z'_i) and (0, y_i, 0), respectively; *t* denotes time; t_i is the time of the plane wave propagating along the x' direction from *j* to *i*; and the superscript (1) denotes the value given in the local coordinate (x', y, z'). The velocity, acceleration and stress can be extended to three dimensions by the same way as the displacement. If the time $t-t_i$ is not at the temporally discrete point, the site response is obtained by the interpolation of those at the two discrete points on both sides of $t-t_i$.

The site response of the node *i* on the artificial boundary in the local coordinate (x', y, z') can be transformed into the global coordinate (x, y, z) by the coordinate transform as

$$\mathbf{u}_{Bi}^{F} = \mathbf{Q}_1\mathbf{u}_{Bi}^{F(1)} \text{ and } \boldsymbol{\sigma}_{Bi}^{F} = \mathbf{Q}_1\boldsymbol{\sigma}_{Bi}^{F(1)}\mathbf{Q}_1^{T} \tag{29}$$

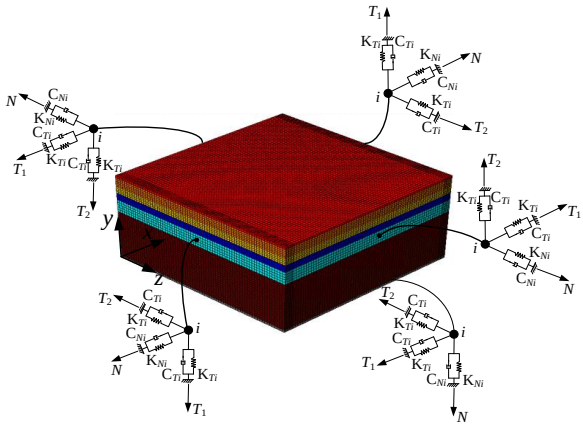

Local coordinate (N,T_1,T_2) for viscous-spring boundary is same as that of representing stress in solid mechanics. N is outward normal of artificial boundary and T is tangential.
For each finite element node on artificial boundary, viscous-spring boundary consists of three lumped parallel spring-dashpot models along three local coordinate axes, respectively.

Fig. 6 Viscous-spring artificial boundary condition

where $\mathbf{u}_{Bi}^{F}$ and $\mathbf{u}_{Bi}^{F(1)}$ are the site displacement vector of the node i in the global and local coordinates, respectively; $\boldsymbol{\sigma}_{Bi}^{F}$ and $\boldsymbol{\sigma}_{Bi}^{F(1)}$ are the site stress matrix of the node i in the global and local coordinates, respectively; and $\mathbf{Q}_1$ is the coordinate transform matrix as

$$\mathbf{Q}_1 = \begin{bmatrix} \cos\varphi & 0 & -\sin\varphi \\ 0 & 1 & 0 \\ \sin\varphi & 0 & \cos\varphi \end{bmatrix} \tag{30}$$

the superscript T denotes the matrix transposition.

Once the free field response on the artificial boundary is obtained by the site response analysis, the seismic load Eq. (6) can be written for the node i as

$$\mathbf{f}_{Bi}^{\infty} = \mathbf{K}_{Bi}^{\infty}\mathbf{u}_{Bi}^{F} + \mathbf{C}_{Bi}^{\infty}\dot{\mathbf{u}}_{Bi}^{F} + \mathbf{f}_{Bi}^{F} \tag{31}$$

with the nodal force obtained from the stress by the lumped finite element discretization along the artificial boundary as

$$\mathbf{f}_{Bi}^{F} = A_i\boldsymbol{\sigma}_{Bi}^{F}\mathbf{d} \tag{32}$$

where $\mathbf{d}$ is the outward normal of the artificial boundary at the node i; and A_i is the area for the node i on the artificial boundary due to the lumped discretization.

5.2 Viscous-spring boundary condition

The viscous-spring boundary (Deeks and Randolph 1994, Du *et al*. 2006, Liu *et al*. 2006, Du and Zhao 2010) is a parallel spring-dashpot model for each degree of freedom on the artificial boundary, as shown in Fig. 6, when the lumped finite element discretization is used. The viscous boundary is a special case of the viscous-spring boundary with the zero spring coefficient. The spring provides the stiffness to avoid the possible zero-frequency instability of the viscous boundary.

5.2.1 Formulation in local coordinate

As shown in Fig. 6, the local coordinate (N, T_1, T_2) is same as that of representing the stress in solid mechanics. N is the outward normal of the artificial boundary and T is the tangential. For the finite element node i on the artificial boundary, the viscous-spring boundary Eq. (4) is given in the local coordinate as

$$\mathbf{f}_{Bi}^{S(2)} = -\mathbf{K}_{Bi}^{\infty(2)}\mathbf{u}_{Bi}^{S(2)} - \mathbf{C}_{Bi}^{\infty(2)}\dot{\mathbf{u}}_{Bi}^{S(2)} \tag{33}$$

where the subscript i denotes the node i; and the superscript (2) denotes the local coordinate (N, T_1, T_2). Three parallel spring-dashpot models are along three local coordinate axes, respectively.

The spring and dashpot matrices can be written, respectively, as

$$\begin{aligned} \mathbf{K}_{Bi}^{\infty(2)} &= A_i\begin{bmatrix} K_{Ni} & 0 & 0 \\ 0 & K_{Ti} & 0 \\ 0 & 0 & K_{Ti} \end{bmatrix}, \\ \mathbf{C}_{Bi}^{\infty(2)} &= A_i\begin{bmatrix} C_{Ni} & 0 & 0 \\ 0 & C_{Ti} & 0 \\ 0 & 0 & C_{Ti} \end{bmatrix} \end{aligned} \tag{34}$$

where A_i is the area for the node i on the artificial boundary due to the lumped discretization; K_{Ni} and K_{Ti} are the normal and tangential spring coefficients, respectively; and C_{Ni} and C_{Ti} are the normal and tangential dashpot coefficients, respectively. The spring and dashpot coefficients are listed in Table 2.

Table 2 Parameters of viscous-spring boundary

	K_{Ni}	K_{Ti}	C_{Ni}	C_{Ti}
Three dimensions	$\frac{4G}{r}$	$\frac{2G}{r}$	ρc_P	ρc_S
Two dimensions	$\frac{2G}{r}$	$\frac{3G}{2r}$	ρc_P	ρc_S

where ρ and G is the mass density and shear modulus of the infinite domain, respectively; c_P and c_S are the P and S wave velocities, respectively; and r is a constant decided by the artificial boundary size that is chosen as the height of the finite element model here. For the layered half space, the different choices of these material constants are discussed in the numerical example.

The viscous-spring boundary is obtained based on the one-dimensional wave theory. They are applied

approximately to the SSI problem especially for the horizontally layered half space site. The choice of the parameters listed in Table 2 is not unique. The effect of the different parameters on the response of the soil-structure system is studied in Section 6.

5.2.2 Formulation in global coordinate

For transforming Eq. (33) from the local coordinate (N, T_1, T_2) to the global coordinate (x, y, z), the following relationship between the vectors in two coordinates is used.

$$\mathbf{f}_{Bi}^{S(2)} = \mathbf{Q}_2 \mathbf{f}_{Bi}^{S}, \quad \mathbf{u}_{Bi}^{S(2)} = \mathbf{Q}_2 \mathbf{u}_{Bi}^{S} \quad \text{and} \quad \dot{\mathbf{u}}_{Bi}^{S(2)} = \mathbf{Q}_2 \dot{\mathbf{u}}_{Bi}^{S} \tag{35}$$

where $\mathbf{Q}_2$ is the coordinate transform matrix, and can be written for the artificial boundary surfaces with the outward normal as positive x direction, negative x direction, positive z direction, negative z direction and negative y direction shown in Fig. 6, respectively, as

$$\mathbf{Q}_2 = \begin{bmatrix} 1 & 0 & 0 \\ 0 & 1 & 0 \\ 0 & 0 & 1 \end{bmatrix}, \quad \mathbf{Q}_2 = \begin{bmatrix} -1 & 0 & 0 \\ 0 & 0 & -1 \\ 0 & -1 & 0 \end{bmatrix}$$

$$\mathbf{Q}_2 = \begin{bmatrix} 0 & 0 & 1 \\ 1 & 0 & 0 \\ 0 & 1 & 0 \end{bmatrix}, \quad \mathbf{Q}_2 = \begin{bmatrix} 0 & 0 & -1 \\ 0 & -1 & 0 \\ -1 & 0 & 0 \end{bmatrix} \tag{36}$$

$$\text{and} \quad \mathbf{Q}_2 = \begin{bmatrix} 0 & -1 & 0 \\ -1 & 0 & 0 \\ 0 & 0 & -1 \end{bmatrix}$$

Substituting Eq. (35) into Eq. (33), and using the orthogonality of the coordinate transform matrix, obtain the viscous-spring boundary in the global coordinate as

$$\mathbf{f}_{Bi}^{S} = -\mathbf{K}_{Bi}^{\infty} \mathbf{u}_{Bi}^{S} - \mathbf{C}_{Bi}^{\infty} \dot{\mathbf{u}}_{Bi}^{S} \tag{37}$$

with the spring and dashpot coefficient matrices in the global coordinate as

$$\mathbf{K}_{Bi}^{\infty} = \mathbf{Q}_2^T \mathbf{K}_{Bi}^{\infty(2)} \mathbf{Q}_2 \quad \text{and} \quad \mathbf{C}_{Bi}^{\infty} = \mathbf{Q}_2^T \mathbf{C}_{Bi}^{\infty(2)} \mathbf{Q}_2 \tag{38}$$

where the superscript T denotes the matrix transposition.

5.3 Initial condition for nonlinear analysis

Eq. (1) can consider the nonlinearity of the finite domain to perform the nonlinear SSI analysis under earthquake. The initial stress due to gravity requires considering. It is obtained by a static analysis before the seismic SSI analysis. In the finite element model of Fig. 3, the normal displacement of the artificial boundary is constrained. The static analysis is performed under gravity. The stress is obtained. The obtained stress and constraint reaction are the initial condition of the SSI analysis under the earthquake and gravity.

6. Verification

6.1 Seismic site response

This subsection verifies the proposed method for the site response from the obliquely incident earthquake and the three-dimensional site response analysis in Subsection 5.1. The Daikai site listed in Table 1 subjected to the earthquake shown in Fig. 5 is analyzed.

In the proposed method, the one-dimensional finite element mesh is same as that along the depth of the artificial boundary of the finite element model shown in Fig. 3. The solutions obtained by the proposed method are shown in Figs. 7 and 8, respectively, for the obliquely incident P wave and SV wave. To demonstrate the effectiveness of the proposed method, the stiffness matrix method (Kausel and Roesset 1981) is used for comparison. It can be seen from the figures that the solutions obtained by the proposed method agree very well with that by the stiffness matrix method. The proposed method can obtain the accurate site response. The solution by the stiffness matrix method has the possible large error from about 0 to 1 s due to the Fourier transform. The proposed method avoid this problem due to that it works in time domain.

The three-dimensional site is further analyzed by the direct method in ABAQUS® subjected to the one-dimensional

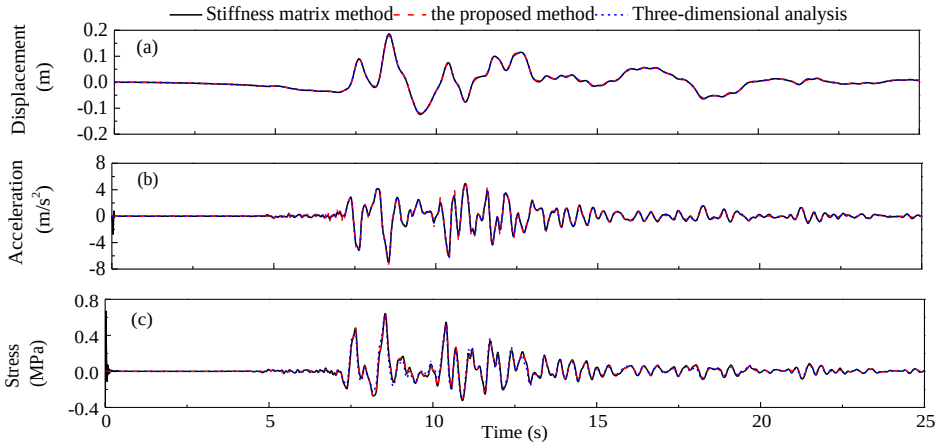

Fig. 7 Site responses from obliquely incident P wave of θ=30° and φ=60°. (a) Displacements and (b) accelerations along y direction at ground surface; and (c) Maximum principal stresses at depth of 40.3 m

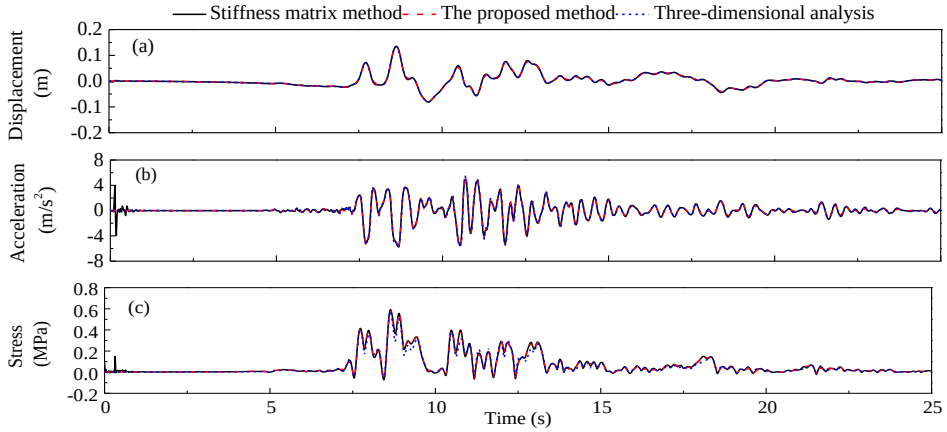

Fig. 8 Site responses from obliquely incident *SV* wave of θ=10° and φ=60°. (a) Displacements and (b) accelerations along *x* direction at ground surface; and (c) Maximum principal stresses at depth of 40.3 m

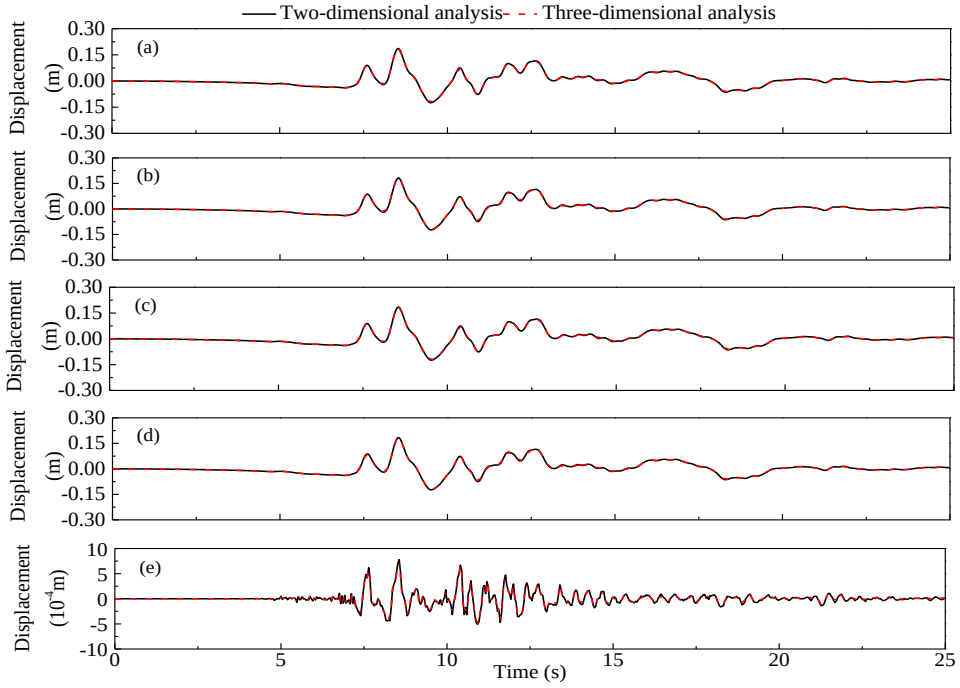

Fig. 9 Soil-structure interactions by two- and three-dimensional analyses from obliquely incident *P* wave of θ=30° and φ=0°. Displacements along *y* direction (a) at depth 4.1 m of left artificial boundary, (b) in the middle of bottom artificial boundary, (c) at depth 4.1 m of right artificial boundary, and (d) in the middle of central column; and (e) Relative displacements along *y* direction between top and bottom of central column

site response obtained by the proposed method. If the extension and input of the site response are right, the three-dimensional site response along *y* axis should agree with the one-dimensional response by the proposed method. The solutions obtained by the three-dimensional analysis are also shown in Figs. 7 and 8. It can be seen that the solutions obtained by the three-dimensional site response analysis agree very well with those by the proposed method.

6.2 Viscous-spring boundary condition

This subsection studies the accuracy of the viscous-spring boundary given in Subsection 5.2. The viscous-spring boundary absorbs the scattered field. It does not affect the results in the free field computation in the above section although it is an approximate method. However, the scattered field exists in the seismic SSI problem. The accuracy of the viscous-spring boundary should be studied in the seismic SSI.

To study the accuracy of the viscous-spring boundary, a finite element model of the sufficiently large finite domain should be used to obtain a reference solution. The location of the truncation boundary in the reference model is chosen according to the finiteness of the wave propagation velocity. The location should assure that the solution at the interested domain is not affected by the fictitious wave arising from the scattered field reflected by the truncation boundary during the analysis. The reference model is so large that its computational cost is not acceptable for the three-dimensional problem. The accuracy of the viscous-spring

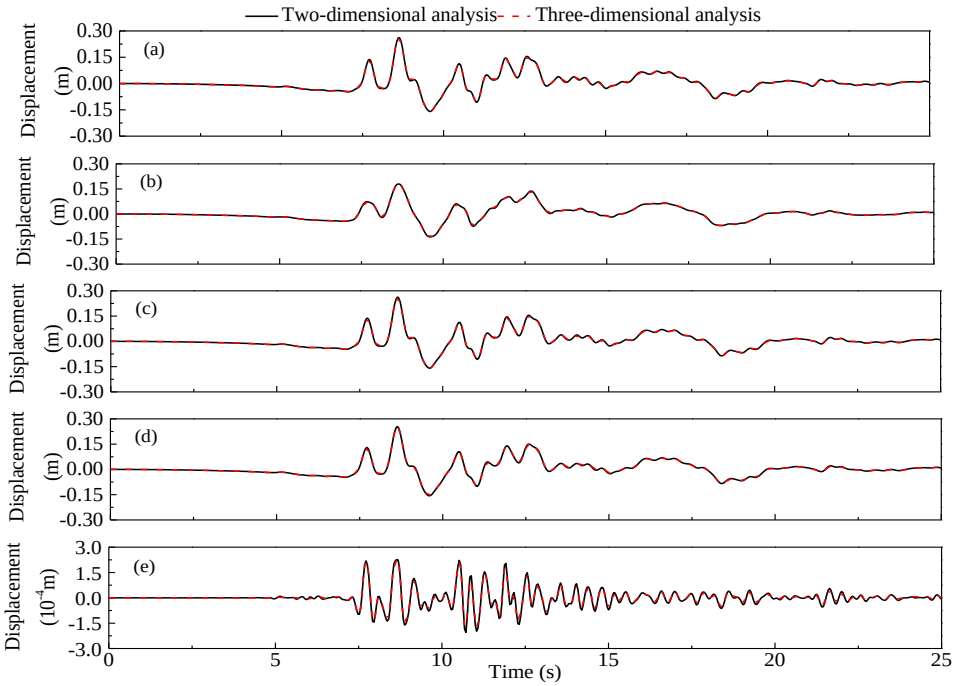

Fig. 10 Soil-structure interactions by two- and three-dimensional analyses from obliquely incident *SV* wave of θ=10° and φ=0°. Displacements along *x* direction (a) at depth 4.1 m of left artificial boundary, (b) in the middle of bottom artificial boundary, (c) at depth 4.1 m of right artificial boundary, and (d) in the middle of central column; and (e) Relative displacements along *x* direction between top and bottom of central column

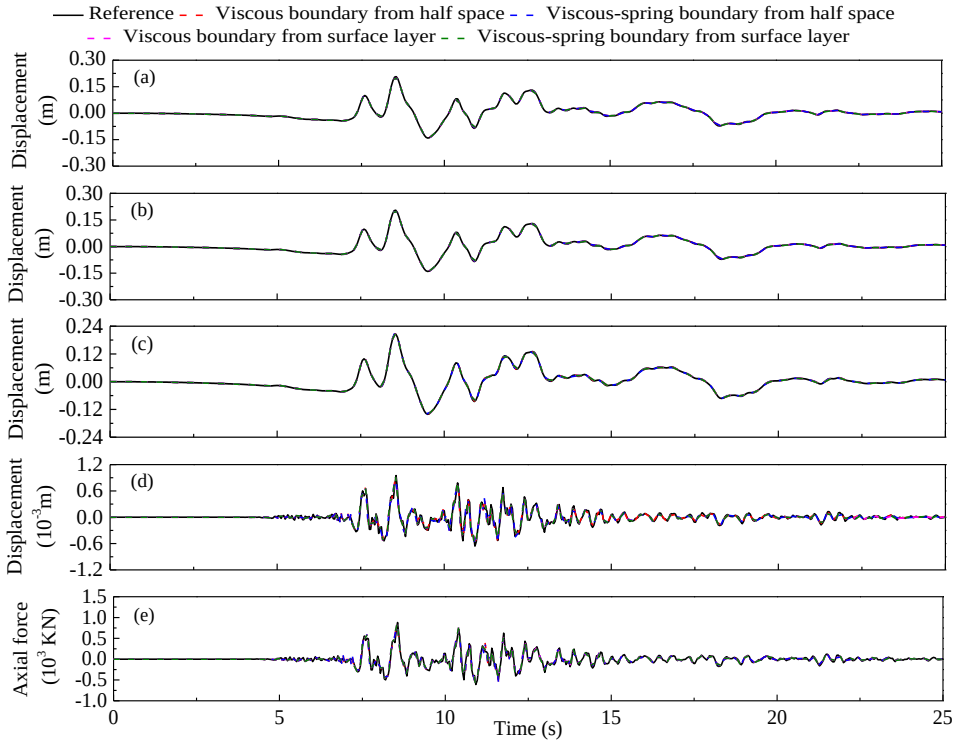

Fig. 11 Two-dimensional soil-structure interactions by viscous-spring boundaries with different parameters from vertically incident *P* wave of θ=0°. Displacements along *y* direction (a) at depth 4.1 m of left artificial boundary, (b) in the middle of bottom artificial boundary, and (c) in the middle of central column; (d) Relative displacements along *y* direction between top and bottom of central column; and (e) Axial forces in the middle of central column. Reference means a finite element model of the sufficiently large finite domain

boundary is therefore studied by the two-dimensional analysis.

The three-dimensional analysis is compared with the two-dimensional one. The three-dimensional analysis

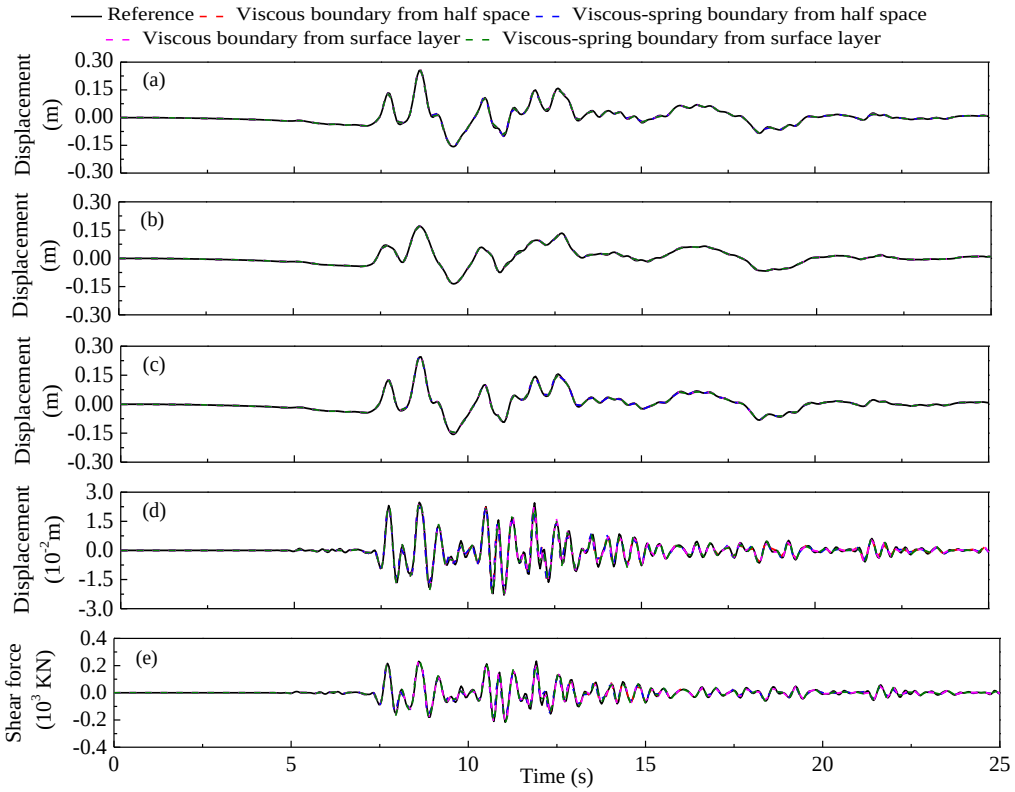

Fig. 12 Two-dimensional soil-structure interactions by viscous-spring boundaries with different parameters from vertically incident SV wave of θ=0°. Displacements along x direction (a) at depth 4.1 m of left artificial boundary, (b) in the middle of bottom artificial boundary, and (c) in the middle of central column; (d) Relative displacements along x direction between top and bottom of central column; and (e) Shear forces in the middle of central column. Reference means a finite element model of the sufficiently large finite domain

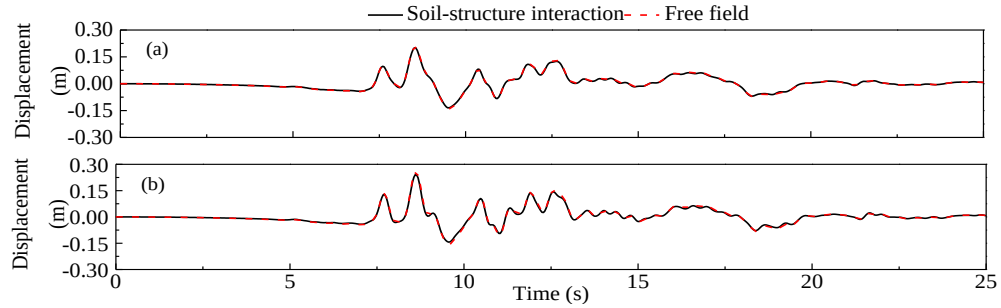

Fig. 13 Comparison between soil-structure interaction and free field. Displacements at depth 4.1 m of left artificial boundary (a) along y direction from vertically incident P wave and (b) along x direction from vertically incident SV wave, respectively

chooses the incident P or SV wave with φ=0°. The solutions in the plane of z=35 m are the adequately accurate plane strain solutions. Two-dimensional analysis performs the plane strain computation directly with the same parameters as the three-dimensional case. The elastic modulus of central column is 1/3.5 of that of concrete in the two-dimensional analysis. The two-dimensional viscous-spring boundary sees Table 2. The parameters of the viscous-spring boundary are determined according to the underlying half space. The results are shown in Figs. 9 and 10. It can be seen from the figures that the two-dimensional solutions agree very well with the three-dimensional ones. This indicates that the accuracy study of the viscous-spring boundary in two dimensions can represent that in three dimensions.

Two-dimensional SSI analysis is performed. The parameters in the viscous-spring boundary are chosen according to the half space and the surface layer, respectively. The solutions are shown in Figs. 11 and 12 where the reference solutions are given. It can be seen from the figures that the solutions obtained by the different viscous-spring boundaries agree very well and all of them agree with the reference solution. This indicates that the viscous-spring boundary have the sufficient accuracy for the seismic SSI and its parameter change does not affect the accuracy considerably. In the radiation problem, the viscous-spring boundary has not such high accuracy and its parameter change affects the accuracy relatively considerably. The reason is that the scattered field is much less than the free is much less than the free field in the

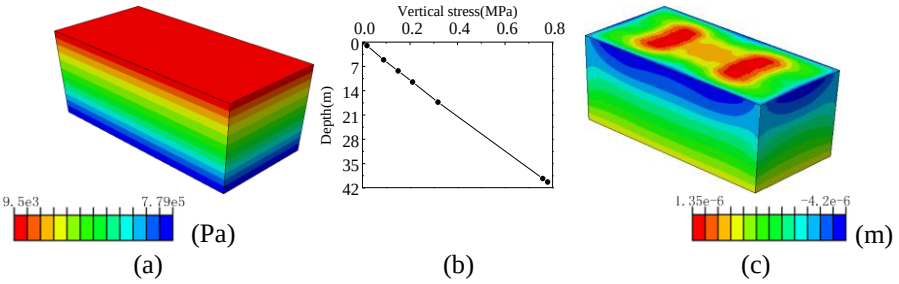

Fig. 14 Initial conditions of free field from gravity. (a) Snapshot of vertical stress; (b) Vertical stress along depth; and (c) Snapshot of vertical displacement

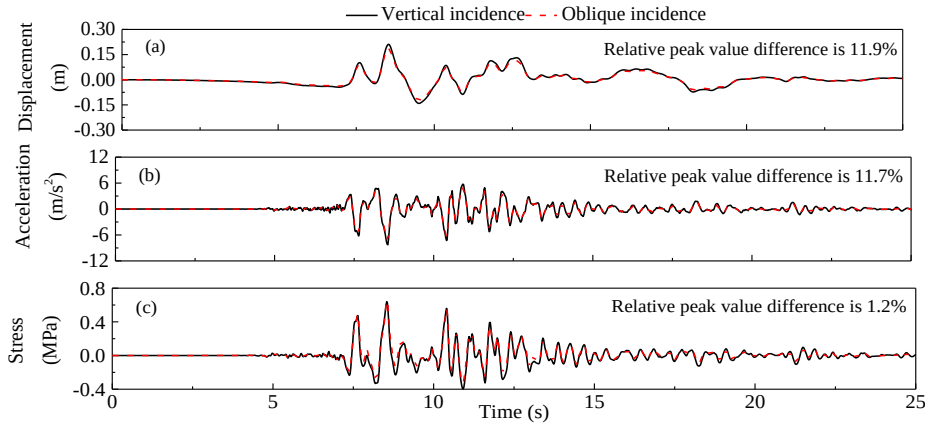

Fig. 15 Site responses from *P* waves of vertical incidence θ=0° and of oblique incidence θ=30° and φ=60°, respectively. (a) Displacements and (b) accelerations along *y* direction at ground surface; and (c) Maximum principal stresses at depth of 40.3 m

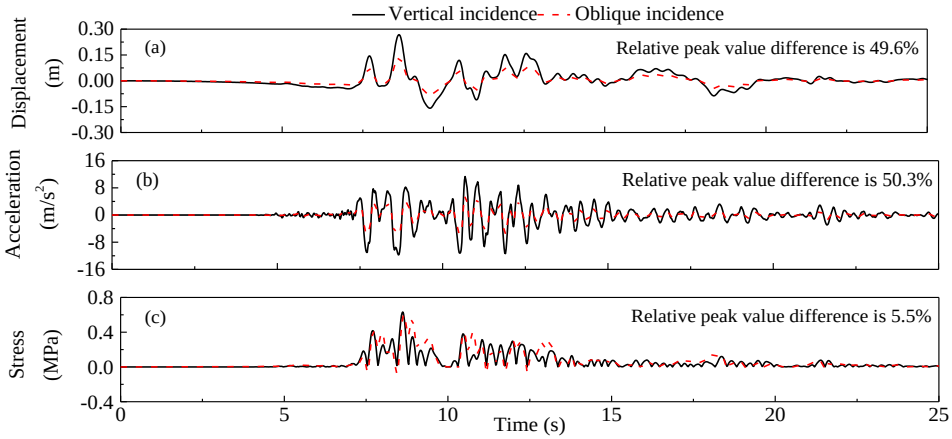

Fig. 16 Site responses from *SV* waves of vertical incidence θ=0° and of oblique incidence θ=10° and φ=60°, respectively. (a) Displacements and (b) accelerations along *x* direction at ground surface; and (c) Maximum principal stresses at depth of 40.3 m

seismic SSI. This can be seen in Fig. 13.

6.3 Initial condition for nonlinear analysis

This subsection verifies the method to compute the initial condition for nonlinear analysis given in Subsection 5.3. The linear Daikai site subjected to gravity is analyzed. The obtained initial condition is applied to a new site model. This new model is computed under gravity. The results are shown in Fig. 14. It can be seen from this figure that the vertical stress is the gravity field and the vertical displacement is nearly zero. This indicates that the initial stress due to gravity is considered but the displacement does not.

7. Effects of obliquely incident earthquake

7.1 Linear site

This subsection gives the effect of the obliquely incident earthquake on the seismic site response. The Daikai site

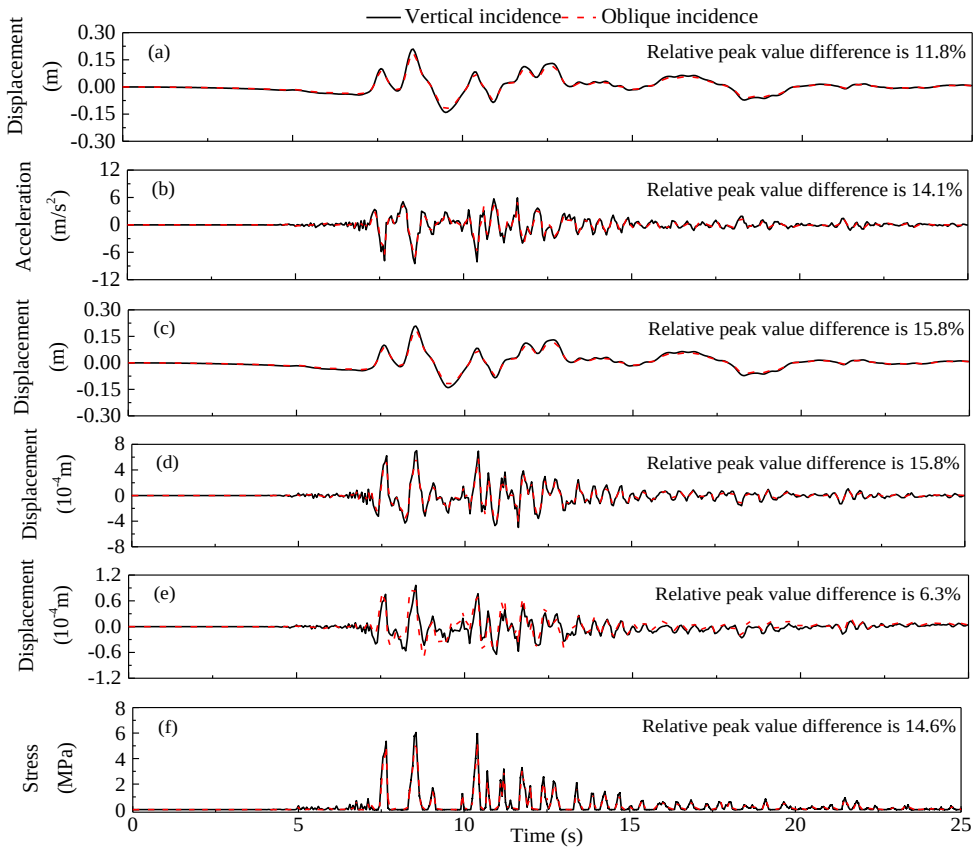

Fig. 17 Linear soil-structure interactions from *P* waves of vertical incidence θ=0° and of oblique incidence θ=30° and φ=60°, respectively. Displacements along *y* direction (a) at ground surface and (c) in the middle of central column; (b) Accelerations along *y* direction at ground surface; Relative displacements along *y* direction between top and bottom (d) of central column and (e) of side wall; and (f) Maximum principal stresses in the middle of central column

responses are shown in Figs. 15 and 16, respectively, from the incident *P* wave and *SV* wave. The relative differences of peak values between the oblique and vertical incidences are given. It can be seen that the effect of the obliquely incident earthquake on the site response is considerable.

7.2 Linear soil-structure interaction

This subsection gives the effect of the obliquely incident earthquake on the linear SSI. The seismic responses of the Daikai subway station system are shown in Figs. 17 and 18, respectively, from the incident *P* wave and *SV* wave. The relative differences of peak values between the oblique and vertical incidences are given. It can be seen that the effect of the obliquely incident earthquake on the linear SSI is considerable.

7.3 Nonlinear soil-structure interaction

This subsection gives the effect of the obliquely incident earthquake on the nonlinear SSI. The finite domain consider material nonlinearity and the truncated soil (infinite domain) is regarded as linear elastic. The material nonlinearity of the soil in finite domain is considered by the Mohr-coulomb model of cohesion stress 20 KPa, friction angle 35 and dilation angle 2. The seismic responses of the Daikai subway station system are shown in Figs. 19 and 20, respectively, from the incident P wave and SV wave. The relative differences of peak values between the oblique and vertical incidences are given. It can be seen that the effect of the obliquely incident earthquake on the nonlinear SSI is considerable.

8. Conclusions

A method is proposed to input the obliquely incident earthquake into the SSI system in the layered half space. It consists of a new site response analysis method for free field and the viscous-spring boundary condition for scattered field.

The site response analysis method is a time-domain one-dimensional finite element method. It has the same accuracy as the classical frequency-domain method such as the stiffness matrix method, and avoids the possible error due to Fourier transform. The approximate viscous-spring boundary condition have the sufficient accuracy and its parameter change does not affect the accuracy considerably, because the scattered field is much less than the free field in the seismic SSI. The proposed earthquake input method can be implemented in the preprocessing of a commercial finite element software. The effects of the obliquely incident earthquake on the response of Daikai site and subway station are considerable. The proposed earthquake input

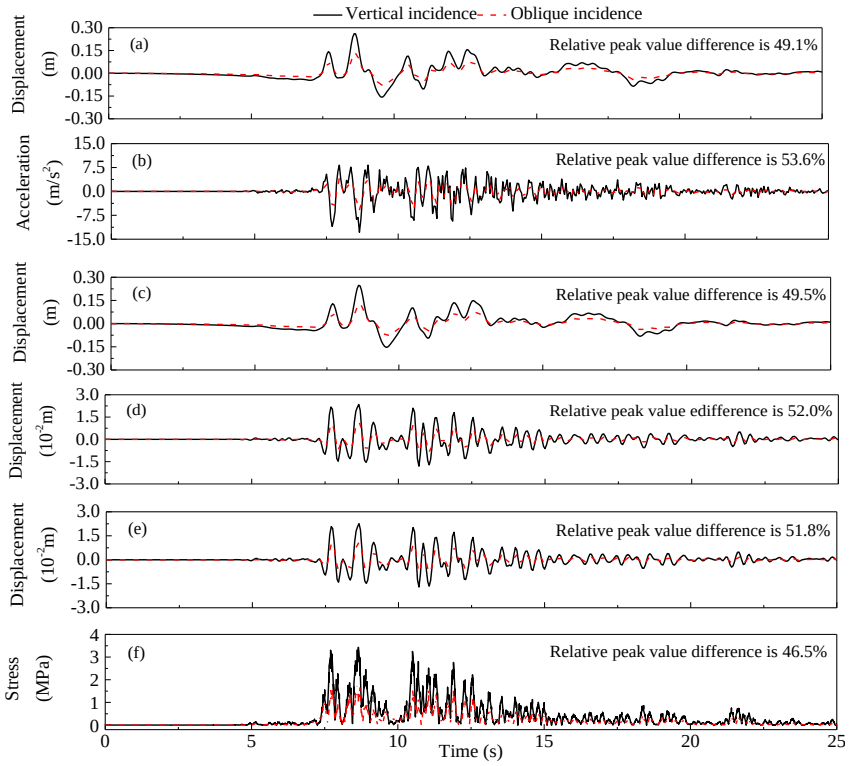

Fig.18 Linear soil-structure interactions from SV waves of vertical incidence θ=0° and of oblique incidence θ=10° and φ=60°, respectively. Displacements along x direction (a) at ground surface and (c) in the middle of central column; (b) Accelerations along x direction at ground surface; Relative displacements along x direction between top and bottom (d) of central column and (e) of side wall; and (f) Maximum principal stresses in the middle of central column

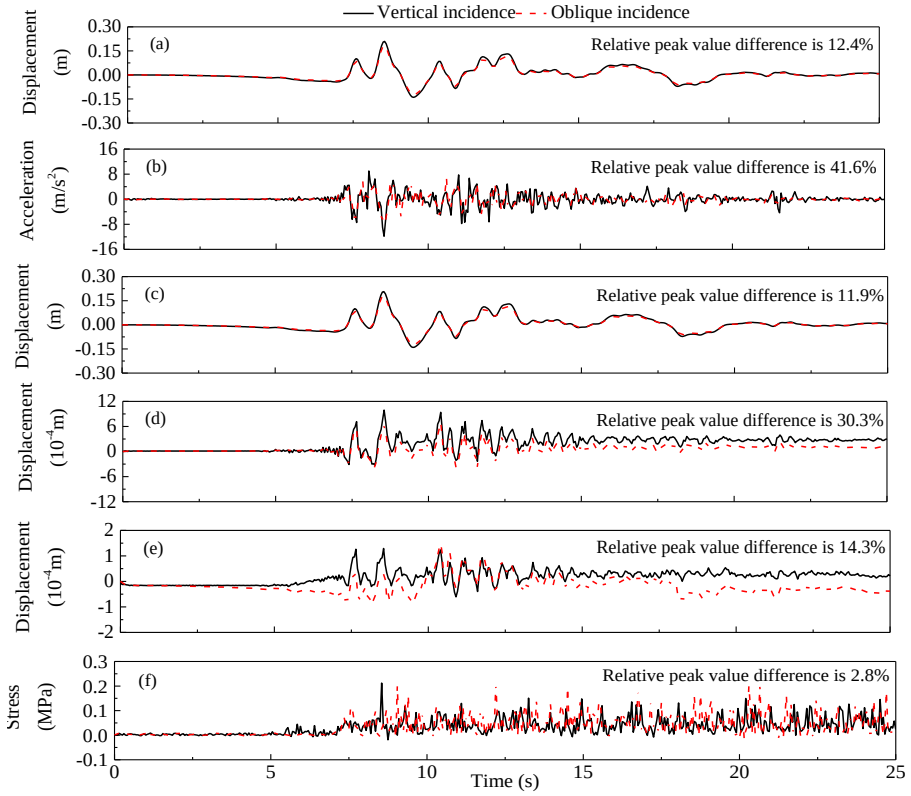

Fig. 19 Nonlinear soil-structure interactions from P waves of vertical incidence θ=0° and of oblique incidence θ=30° and φ=60°, respectively. Displacements along y direction (a) at ground surface and (c) in the middle of central column; (b) Accelerations along y direction at ground surface; Relative displacements along y direction between top and bottom (d) of central column and (e) of side wall; and (f) Maximum principal stresses in the middle of central column

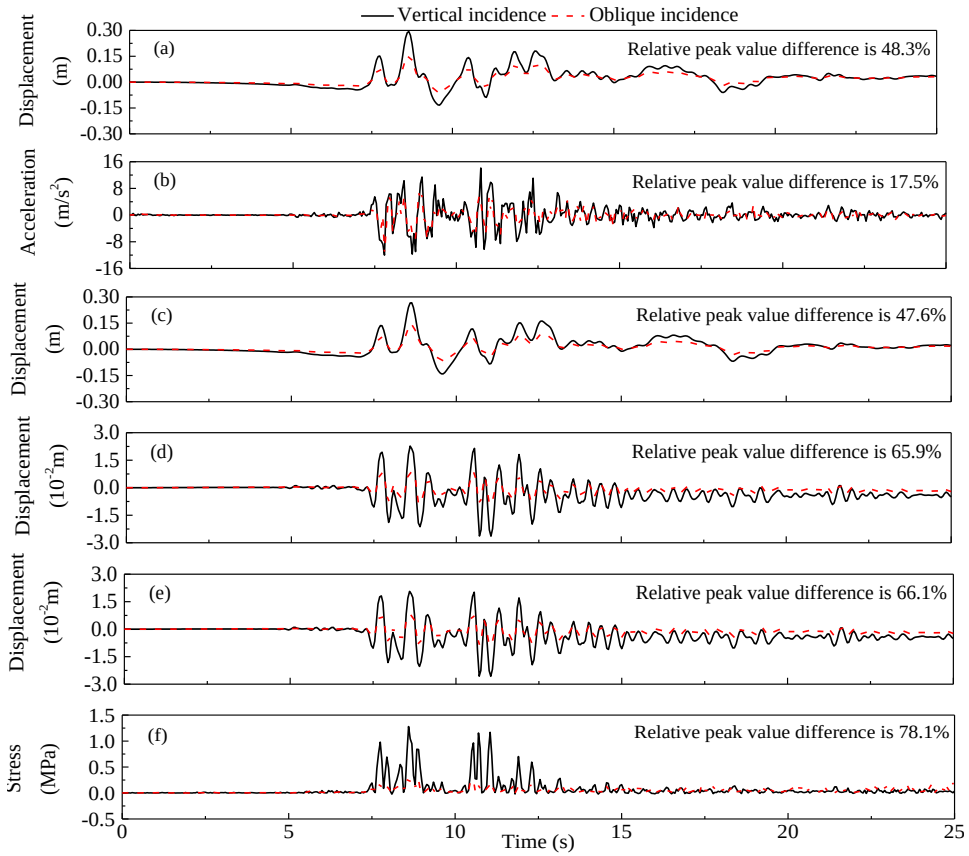

Fig. 20 Nonlinear soil-structure interactions from SV waves of vertical incidence θ=0° and of oblique incidence θ=10° and φ=60°, respectively. Displacements along x direction (a) at ground surface and (c) in the middle of central column; (b) Accelerations along x direction at ground surface; Relative displacements along x direction between top and bottom (d) of central column and (e) of side wall; and (f) Maximum principal stresses in the middle of central column

method can also be applied to the seismic SSI analysis of the other structure. The truncated soil is assumed as linear elasticity in the present work. The nonlinearity of the truncated soil should be considered in the future.

Acknowledgements

This work is supported by National Basic Research Program of China (2015CB057902), and National Natural Science Foundation of China (51421005, 51678015, 51578513 and 51322813).

References

ABAQUS/Standard User's Manual Version 5.8 (1998), Hibbit, Karlsson Sorensen Inc., USA.

Fast lagrangian analysis of continua version 4.0. (2000).

An, X.H., Shawky, A.A. and Maekawa, K. (1997a), "The collapse mechanism of a subway during the Great Hanshin earthquake", *Cement Concrete Compos.*, **19**(3), 241-257.

An, X., Shawky A.A. and Maekawa, K. (1997b), "The collapse mechanism of a subway station during the Great Hanshin earthquake", *Cement Concrete Compos.*, **19**, 241-57.

Berenger, J.P. (1994), "A perfectly matched layer for the absorption of electromagnetic waves", *J. Comput. Phys.*, **114**(2), 185-200.

Birk, C. and Behnke, R. (2012), "A modified scaled boundary finite element method for three-dimensional dynamic soil-structure interaction in layered soil", *Int. J. Numer. Meth. Eng.*, **89**(3), 371-402.

Chen, S., Tang, G., Liu, Q. and Ding, H. (2010), "A direct time-domain method for analysis of three-dimensional soil-structure dynamic interaction", *Earthq. Eng. Eng. Vib.*, **30**(2), 24-31. (in Chinese)

Chen, X.J., Birk, C. and Song, C. (2015), "Time-domain analysis of wave propagation in 3-D unbounded domains by the scaled boundary finite element method", *Soil Dyn. Earthq. Eng.*, **75**, 171- 182.

Deeks, A.J. and Randolph, M.F. (1994), "Axisymmetric time-domain transmitting boundaries", *Am. Soc. Civil Eng.*, **120**(1), 25-42.

Du, X.L. and Zhao, M. (2010), "Stability and identification for rational approximation of frequency response function of unbounded soil", *Earthq. Eng. Struct. Dyn.*, **39**(2), 165-186.

Du, X.L., Zhao, M. and Wang, J.T. (2006), "A stress artificial boundary in FEA for near-field wave problem", *Chin. J. Theor. Appl. Mech.*, **38**(1), 49-56.

Du, X.L. and Zhao, M. (2010), "A local time-domain transmitting boundary for simulating cylindrical elastic wave propagation in infinite media", *Soil Dyn. Earthq. Eng.*, **30**(10), 937-946.

Galvín, P. and Romero, A. (2014), "A MATLAB toolbox for soil-structure interaction analysis with finite and boundary elements", *Soil Dyn. Earthq. Eng.*, **57**(2), 10-14.

Ghandil, M. and Behnamfar, F. (2015), "The near-field method for dynamic analysis of structures on soft soils including inelastic soil-structure interaction", *Soil Dyn. Earthq. Eng.*, **75**, 1-17.

Givoli, D. (1999), "Recent advances in the DtN FE method". *Arch. Comput. Meth. Eng.*, **2**(6), 71-116.
Givoli, D. (2004), "High-order local non-reflecting boundary conditions: a review", *Wave Motion*, **4**(39), 319-326.
Hall, W.S. and Oliveto, G. (2009), *Boundary Element Methods for Soil-Structure Interaction*, Springer Netherlands.
Haskell, N.A. (1951), "The dispersion of surface waves on multilayered media", *Bull. Seismol. Soc. Am.*, **43**(1), 17-34.
Hudson, M., Idriss, I.M. and Beikae, M. (2003), User's Manual for QUAD4M.
Kausel, E. (1994), "Thin-layer method: formulation in the time domain", *Int. J. Numer. Meth. Eng.*, **37**(6), 927-941.
Kausel, E. and Roesset, J.M. (1981), "Stiffness matrices for layered soils", *Bull. Seismol. Soc. Am.*, **6**(71), 1743-1761.
Liao, Z.P. (1996), "Extrapolation nonreflecting boundary conditions", *Wave Motion*, **24**, 117-138.
Liao, Z.P. and Wong, H.L. (1984), "A transmitting boundary for the numerical simulation of elastic wave propagation", *Soil Dyn. Earthq. Eng*., **84**(3).
Liu, J.B., Du, Y.X., Du, X.L., Wang, Z.Y. and Wu, J. (2006), "3D viscous-spring artif icial boundary in time domain", *Earthq. Eng. Eng. Vib*., **1**(5), 93-101.
Liu, J.B. and Wang, Y. (2006), "A 1D time-domain method for out-Plane wave motions in a layered half-space", *Chin. J. Theor. Appl. Mech.*, **2**(38), 219-225.
Liu, J.B. and Wang, Y. (2007), "A 1D time-domain method for in-Plane wave motions in a layered half-space", *Eng. Mech.*, **27**(7), 16-22.
Lysmer, J. (1969), "Finite dynamic model for infinite media", *J. Eng. Mech. Div.*, **95**, 859-878.
Lysmer, J., Ostadan, F. and Tabatabaie, M. (2000), SASSI: A System for Analysis of Soil-Structure Interaction, CA.
Lysmer, J., Udaka, T., Tsai, C. and Seed, H.B. (1975), *FLUSH a Computer Program for Approximate 3-D Analysis of Soil-Structure Interaction Problems.*
Nielsen, A.H. (2006), "Absorbing boundary conditions for seismic analysis in ABAQUS", *2006 ABAQUS Users' Conference*, 359-376.
Parra-Montesinos, G.J., Bobet, A. and Ramirez, J.A. (2006), "Evaluation of soil-structure interaction and structural collapse in Daikai subway station during Kobe earthquake", *ACI Struct. J.*, **103**(1), 113.
Saouma, V., Miura, F., Lebon, G. and Yagome, Y. (2011), "A simplified 3D model for soil-structure interaction with radiation damping and free field input", *Bull. Earthq. Eng.*, **5**(9), 1387-1402.
Song, C.M. and Wolf, J.P. (1997), "The scaled boundary finite-element method-alias consistent infinitesimal finite-element cell method-for elastodynamics", *Comput. Meth. Appl. Mech. Eng.*, **97**(147), 329-355.
Sun, L. and Pan, Y. (2013), "High-order thin layer method for viscoelastic wave propagation in stratified media", *Comput. Meth. Appl. Mech. Eng.*, **257**(257), 65-76.
Takano, S., Yasui, Y. and Takeda, T. (1988), "The new method to calculate the response of layered half-space subjected to obliquely incident body wave", *Proceeding of Ninth World Conference on Earthquake Engineering*, Tokyo-Kyoto, Japan.
Thomson, W.T. (1950), "Transmission of elastic waves through a stratified solid medium", *J. Appl. Phys.*, **2**(21), 89-93.
Wolf, J.P. (1985), *Dynamic Soil-Structure Interaction*, Prentice Hall, New Jersey.
Wolf, J.P. (1988), *Soil-Structure-Interaction Analysis in Time Domain*, Prentice Hall, New Jersey.
Wolf, J.P. (2003), *The Scaled Boundary Finite Element Method*, John Wiley & Sons Inc.
Wolf, J.P. and Obernhuber, P. (1982), "Free-field response from inclined SH-waves and LOVE-waves", *Earthq. Eng. Struct. Dyn.*, **10**, 823-845.
Wolf, J.P. and Obernhuber, P. (1982), "Free-field response from inclined SV- and P-waves and RAYLEIGH-waves", *Earthq. Eng. Struct. Dyn.*, **10**, 847-869.
Wolf, J.P. and Obernhuber, P. (1983), "In-plane free-field response of actual sites", *Earthq. Eng. Struct. Dyn.*, **11**, 121-134.
Zhang, C., Chen, X. and Wang, G. (1999), "A coupling model of FE-BE-IE-IBE for non-linear layered soil-structure interactions", *Earthq. Eng. Struct. Dyn.*, **28**, 421-441.
Zhang, X., Wegner, J. and Haddow, J. (1999), "Three-dimensional dynamic soil-structure interactions analysis in the time domain", *Earthq. Eng. Struct. Dyn.*, **28**, 1501-1524.
Zhao, C.B. (2009), *Dynamic and Transient Infinite Elements: Theory and Geophysical, Geotechnical and Geoenvironmental Applications*, Spinger, Berlin.
Zhao, M. (2011), "Explicit finite element artificial boundary scheme for transient scalar waves in two-dimensional unbounded waveguide", *Int. J. Numer. Meth. Eng.*, **11**(87), 1074-1104.
Zhao, M., Yin, H., Du, X.L., Liu, J.B. and Liang, L. (2015), "1D finite element artificial boundary method for layered half space site response from obliquely incident earthquake", *Earthq. Struct.*, **1**(9), 173-194.
Zhuang, H.Y., Hu, Z.H., Wang, X.J. and Chen, G.X. (2015), "Seismic responses of a large underground structure in liquefied soils by FEM numerical modeling", *Bull. Earthq. Earthq. Eng.*, **13**(12), 3645-3668

CC